Journal of Power Sources 196 (2011) 5538–5545

Contents lists available at ScienceDirect

Journal of Power Sources

journal homepage: www.elsevier.com/locate/jpowsour

Degradation effects at the methanol inlet, outlet and center region of a stack MEA operated in DMFC

D. Dixon [a,*], K. Wippermann [b], J. Mergel [b], A. Schoekel [a], S. Zils [a], C. Roth [a]

[a] Institute for Materials Science, Technische Universität Darmstadt, Petersenstrasse 23, 64287 Germany
[b] Institute of Energy Research, IEF-3: Fuel Cells, Forschungszentrum Jülich GmbH, 52425 Jülich, Germany

ARTICLE INFO

Article history:
Received 6 October 2010
Received in revised form 21 January 2011
Accepted 2 February 2011
Available online 22 February 2011

Keywords:
Degradation
DMFC
Ru dissolution
Area-specific
Inlet
Outlet
Stack MEA

ABSTRACT

Ru dissolution is one of the key issues in direct methanol fuel cells (DMFC). A used DMFC stack membrane electrode assembly (MEA) was analyzed using different analytical techniques like X-ray diffraction (XRD), X-ray absorption spectroscopy (XAS), transmission electron microscopy (TEM) and EDX and different regions probed in the process. Catalyst powder from e.g. like methanol inlet, outlet and center were investigated and compared with the as-received commercial electrocatalyst and the pristine MEA after manufacture. The large oxidized ruthenium fraction in the anode catalyst was found to play a significant role in particle growth and ruthenium dissolution. Crossover ruthenium from the anode side was found to be dispersed everywhere in the cathode in its oxidized form, and thus can have a significant effect on the oxygen reduction activity (ORR). Although with XRD no significant structural changes were observed for the different regions of the MEA, TEM and EDX analysis showed the preferential precipitation of the Ru at the methanol outlet.

1. Introduction

Direct methanol fuel cells (DMFC) are very efficient and environmentally benign energy converters, which can be implemented in portable, stationary and even mobile appliance systems. Intense scientific research has been invested in understanding these fuel cell systems in recent years. But even though they made an early entry into the market, frequent problems in DMFC like Ru dissolution [1] and methanol cross over need to be addressed [2,3]. Apart from the loss of electrochemical active surface area (ECSA) of anode and cathode due to particle growth and agglomeration [4,5], Ru dissolution from the anode side also plays a major role in catalyst degradation in DMFC. Ru in a Pt/Ru alloy system is known to enhance the methanol oxidation by adsorption of OH and stripping off strongly adsorbed CO from nearby Pt sites [6]. Hence, Ru dissolution can greatly affect the activity of the anode catalyst [7]. It was also found that Ru crossover from the anode can reduce the oxygen reduction reaction activity (ORR) at the cathode as well as affect the sensitivity of the catalyst to cross over methanol [1]. As already discussed plenty in the literature, the Pt/Ru system is often associated with only small amounts of a true alloyed phase, but a large fraction of oxidized ruthenium, which is more prone to dissolution. Rolison et al. predicted that only 25% of the total Ru is actually alloyed with Pt, while the rest is oxidized [8]. These large fractions of oxidized ruthenium preferably in its hydrous form were found to activate the methanol oxidation. In recent work, Saida et al. explained the importance of the morphology and amount of ruthenium oxide on the methanol oxidation activity of a Pt/C catalyst [9]. Although a major fraction of ruthenium oxide is expected to become reduced in DMFC conditions, a minor non-reduced amount can influence the methanol oxidation and ruthenium cross over [1]. Enhanced Ru dissolution is predominantly observed during operating conditions specific to automotive operation like start–stop and fuel starvation, during which the anodic potential rises and facilitates the formation of more ruthenium oxide [10].

In our present study we focus on the detailed and area-selective investigation of catalyst degradation in a membrane electrode assembly (MEA) operated in a fuel cell stack in DMFC mode. The investigation of a real stack MEA is extremely important, as it represents a true system for practical application. Various analytical techniques like XRD, TEM, XAS, and EDX were combined to get a more detailed insight into the distribution of Ru in the degraded device.

2. Experimental

Membrane electrode assemblies were prepared by a knife coating technique. 60% PtRu (Hi Spec 10.000) and 60% Pt (Hi Spec

* Corresponding author. Tel.: +49 6151165498; fax: +49 6151166023.
E-mail address: ditty@energy.tu-darmstadt.de (D. Dixon).

0378-7753/$ – see front matter © 2011 Elsevier B.V. All rights reserved.
doi:10.1016/j.jpowsour.2011.02.007

9.000) was purchased from Johnson Matthey. An ink was prepared from the respective catalysts, knife coated onto carbon cloth GDL material and subsequently hot pressed (135 °C for 3 min) onto a Nafion® 115 membrane. The fuel cell stack was operated in a test rig environment and in a DMFC system [11]. There was alternating operation and standstill for more than 5000 h. The load during operation was at a current density in the range of 50–120 mA/cm^2 and at a temperature range from 40 to 70 °C but mainly at 60 °C. Different regions of the 'end of life' (EOL) MEA from the anode side (methanol inlet, outlet and middle) and the cathode (oxygen inlet, outlet and middle) were analyzed using various analytical techniques and compared with a pristine MEA and the as-received catalysts.

There are several differences between the operation in a test rig and a system. The main point is that in the system there is no possibility for external heating of the stack. This means that the stack is operated at a lower temperature level than in the test rig. The chance of failures in system components and operating conditions is higher than in test rig operation. In system operation, the anodic water is recycled and the operation media (air and methanol) may be contaminated with impurities, which can accumulate in the stack. Also it is likely that there is methanol depletion during standstill. This can accelerate the corrosion of ruthenium.

2.1. XRD

X-ray diffraction was performed on catalyst powder carefully scratched off from the MEA from different regions and analyzed using a STOE STADI-P diffractometer with germanium monochromized Cu K_α radiation in transmission geometry. The XRD patterns were measured between 30° and 90° in 2θ and refined using FULLPROF suit package. Subsequently, they were analyzed for particle size using the Scherrer equation [12].

2.2. EXAFS

All EXAFS data were recorded at beamline X1, Hasylab in transmission geometry. Si (1 1 1) and Si (3 1 1) monochromized beam was used to record the Pt L_3 and Ru K edge spectra respectively. In situ DMFC measurements were carried out using a fuel cell modified for XAS measurements previously reported elsewhere [13]. XAS data were then processed by the ATHENA code [14]. The raw spectra were calibrated and subsequently background corrected using the Autobk algorithm reported elsewhere [15]. The background corrected spectra were normalized in the EXAFS range of 150–1000 eV. The EXAFS fitting analysis was done on the processed data using ARTEMIS [13]. At each edge, three different scattering paths were used (Pt–Pt, Pt–Ru, Pt–O and Ru–Pt, Ru–Ru, Ru–O) to fit the data with a model. All the fits were done in R space with k^2 weighting. To get a reasonable comparison of the coordination numbers the Debye Waller factor was fixed at 0.005 and the amplitude reduction factor was set to 0.934 for Pt and to 0.916 for Ru, as reported in the literature [16].

2.3. Electron microscopy

For the transmission electron microscopy (TEM) investigations ultra microtome sample preparation was performed using a procedure developed by Blom et al. [17]. After carefully removing the gas diffusion layer (GDL) from the MEA, a knife cut thin specimen was made from different regions and embedded in Araldite 502 resin (SPI Supplies, Inc.). This sample was cured for about 16 h at 60 °C, before thin cuts of 200 nm and 70 nm thickness were sliced using a Reichert–Jung ultracut microtome. 70 nm thick samples were then employed for TEM investigation for high resolution imaging using a Philips CM20 TEM with an acceleration voltage of 200 kV and LaB_6 cathode. EDX mapping analyses were carried out on 200 nm thick samples using a Zeiss 962 scanning electron microscope equipped with an energy dispersive X-ray detector for elemental analysis and mapping.

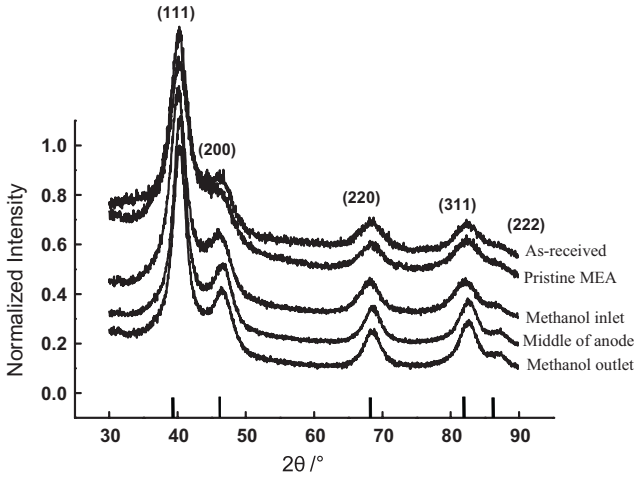

Fig. 1. XRD patterns of the anode catalyst: (a) as-received catalyst, (b) pristine MEA, (c) methanol inlet, (d) anode middle, and (e) methanol outlet, No significant differences are observed for the different anode regions after operation.

3. Results

XRD investigations of the as-received anode catalyst showed Pt reflections shifted to higher 2θ values strongly supporting an alloyed nature in the crystalline fraction of the catalyst [18]. The absence of any Ru reflections in the pattern (Fig. 1) gave strong evidence for the absence of crystalline Ru particles [19]. Table 1 shows the average particle size obtained for the anode catalyst from XRD after Rietveld refinement. No significant particle growth was observed for the anode catalyst in contrast to the cathode catalyst, in which particle growth from 2 nm to 4 nm was observed during the MEA preparation. This pronounced particle growth in the cathode during MEA fabrication might be due to the following reason: as it will be reported later, the anode catalyst contains both X-ray amorphous PtO_2 and RuO_2 phase (cannot be observed by XRD). It is proposed that RuO_2 is more difficult to reduce during the sample preparation compared to PtO_2. The amorphous ruthenium oxide present in the sample may thus act as a dispersion agent and prevent particle growth at the anode side [20]. The aged anode catalyst showed a slight increase in the particle size, but no significant structural differences observed for the different electrode regions. The alloyed nature of the nanoparticles was still pronounced even in the EOL sample. For the cathode catalyst, the particle size was also found to increase with fuel cell operation, but no significant difference in size was observed for the different regions (Table 1). Similar to the aged anode also the XRD patterns (Fig. 2) of the aged cathode catalyst did not show any presence of a crystalline Ru phase caused by Ru dissolution from the anode and cross over to the cathode side.

Table 1
Average particle sizes determined from XRD analysis using the Scherrer equation.

	Particle size (nm)	
	Anode (A)	Cathode (C)
As-received	1.8	2.0
Pristine MEA	1.6	4.0
Inlet	2.3	5.2
Middle	2.3	5.0
Outlet	2.4	5.0

Table 2a
EXAFS analysis of the anode catalyst at the Ru *K* edge.

Ru edge	NRu–Pt	rRu–Pt (Å)	E_0Ru–Pt (eV)	NRu–Ru	rRu–Ru (Å)	E_0Ru–Ru (eV)	NRu–O	rRu–O (Å)	E_0Ru–O (eV)
As-received	1.7	2.72	−7.42	1.6	2.66	−2.68	2.2	1.98	−2.80
Pristine MEA	1.7	2.72	−4.72	1.5	2.67	−2.07	2.1	1.98	−2.05
OCV	1.7	2.70	−8.17	2.4	2.65	−6.90	0.8	2.03	3.93
Inlet	2.8	2.72	−5.68	2.5	2.67	−4.54	1.4	1.99	−0.91
Middle	2.8	2.72	−2.49	2.2	2.65	−7.10	1.4	1.97	−0.87
Outlet	2.5	2.72	−5.30	2.2	2.67	−5.90	1.4	1.95	−3.12

The absolute errors are in the order of 10% for *N* and *E*0 and ±0.02 for *r*. The Debye–Waller factor has been kept constant at 0.005 for all fitting.

Table 2b
EXAFS analysis of the anode catalyst at the Pt L_3 edge.

Pt edge	NPt–Pt	rPt–Pt (Å)	E_0Pt–Pt (eV)	NPt–Ru	rPt–Ru (Å)	E_0Pt–Ru (eV)	NPt–O	rPt-O (Å)	E_0Pt–O (eV)
As-received	3.0	2.72	4.99	1.8	2.72	7.57	1.0	2.00	6.62
Pristine MEA	3.2	2.71	4.61	1.9	2.71	8.80	0.9	1.94	−0.61
Inlet	4.4	2.73	5.04	2.2	2.72	6.58	0.5	1.95	−0.55
Middle	4.4	2.73	4.61	2.2	2.72	7.00	0.5	1.99	2.11
Outlet	4.2	2.73	3.44	2.1	2.72	6.46	0.5	2.00	4.88

However, cross over Ru might be present in an X-ray amorphous state.

Fig. 3a and b represents the Fourier transform spectra of the Pt L_3 and Ru *K* edge data for the commercial anode catalyst powders before and after operation and the fresh MEAs. The broad peaks between 1 and 2 Å are an indication of oxidation in the catalyst. Tables 2a and 2b give a complete overview of the EXAFS results after first shell fitting at both the Ru *K* edge and the Pt L_3 edge. No significant change in the total coordination number (sum of N_{Pt-Pt}, N_{Pt-Ru} and N_{Pt-O}) was observed for the as-received anode catalyst and the fresh MEA strongly supporting XRD findings of no significant particle growth during MEA preparation, since the coordination number can be correlated to the particle size [21]. The Fourier transforms (FT) of both the Pt and Ru edges (Fig. 3a and b) revealed a splitting in the peaks indicating the existence of Pt/Ru alloy [22]. We assume that due to the oxidized Ru present in the catalyst the Pt:Ru ratio greatly deviates from the expected 2:1, and now a random alloy is expected with a larger fraction of Pt.

For the interpretation of the EXAFS data, we propose the existence of 3 different ruthenium phases: Ru in a Pt–Ru alloy, Ru oxide and separate metallic Ru, both X-ray amorphous. The in situ DMFC Ru *K* edge XAS measurements at open circuit potential (OCV) conditions revealed that a significant amount of the ruthenium oxides becomes reduced (N_{Ru-O} = 2.2–0.8), and a corresponding increase in N_{Ru-Ru} (1.5–2.5). Since the number of Pt–Ru nearest neighbours remains constant an increase in the unalloyed, separate Ru is proposed. The reduction of N_{Ru-O} had no significant effect on the N_{Ru-Pt}, which means that the reduced oxide stays unalloyed. Fig. 4 shows the Ru *K* edge FT at OCV. The increase in the FT amplitude around 2.5 Å compared to the fresh catalyst might be due to reduction of some Ru oxides to metallic Ru. It can be observed that the alloyed nature of the anode catalyst is maintained during the whole life time of the MEA, even after a significant fraction of metallic Ru was observed at the cathode (below). To account for the Ru observed at

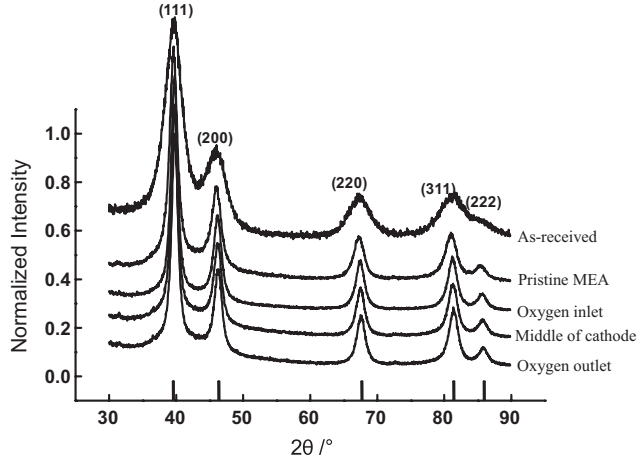

Fig. 2. XRD patterns of the cathode catalyst: (a) as-received catalyst, (b) pristine MEA, (c) oxygen inlet, (d) cathode middle, and (e) oxygen outlet. Particle size is doubled by the MEA fabrication process, but no differences depending on cathode area were observed after operation.

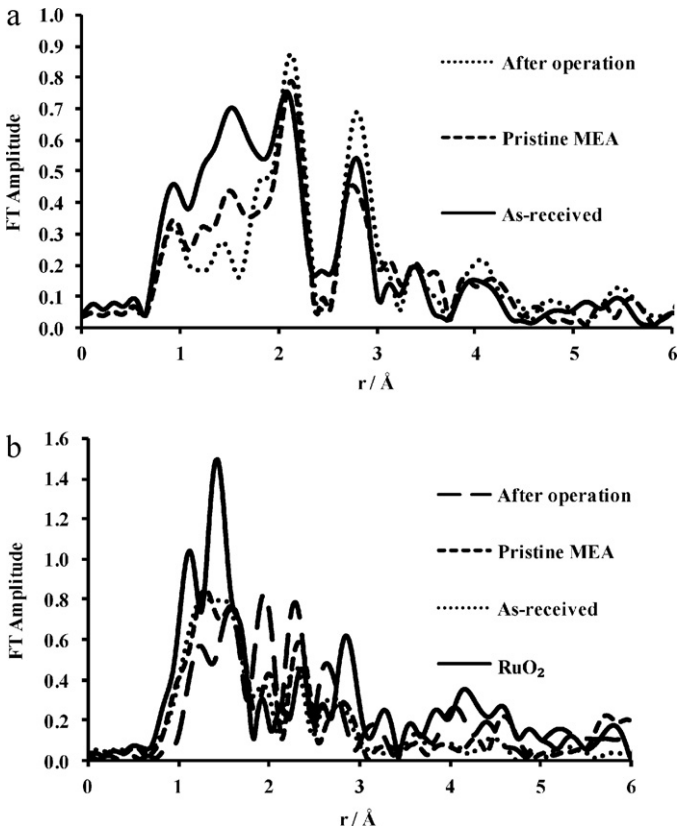

Fig. 3. (a) FT Pt L_3 edge taken for the as-received Pt/Ru catalyst, pristine MEA, and the catalyst powder after operation, (b) FT Ru *K* edge taken for the as-received Pt/Ru catalyst, pristine MEA, the catalyst after operation and a hydrous ruthenium oxide standard. Before operation, ruthenium appears to be largely oxidized.

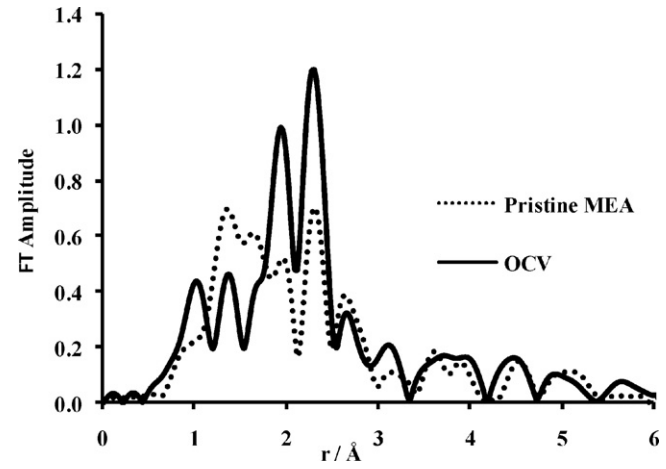

Fig. 4. FT Ru *K* edge spectrum of the pristine MEA compared to the MEA during open circuit voltage (OCV) condition. At OCV, a significant fraction of the Ru oxides gets reduced.

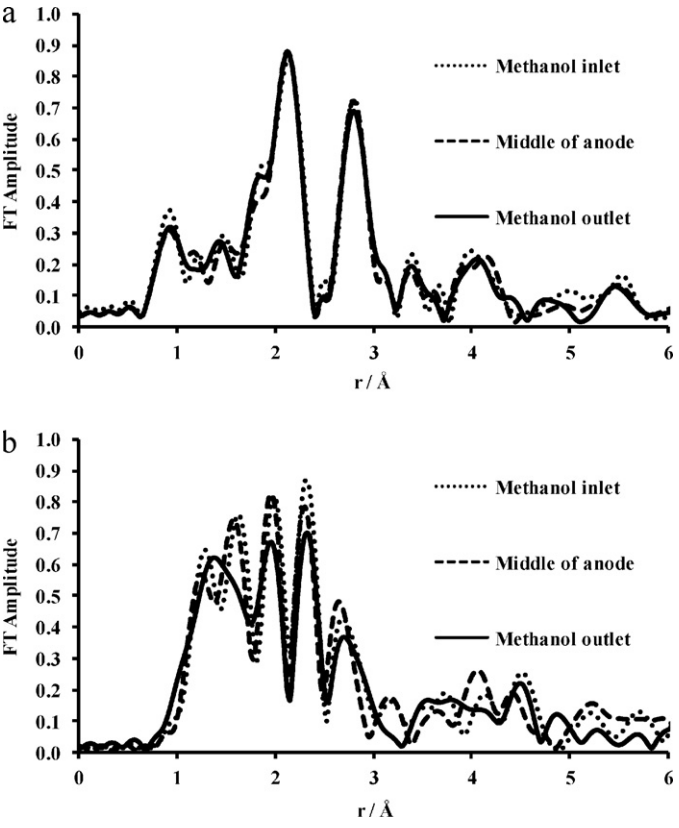

Fig. 5. (a) FT Pt L_3 edge of the anode side taken for the methanol inlet, middle and outlet regions. (b) FT Ru *K* edge of the anode side taken for methanol inlet, middle and outlet regions. While the Pt edge does not show pronounced differences, at the Ru edge the catalyst at the methanol outlet is affected.

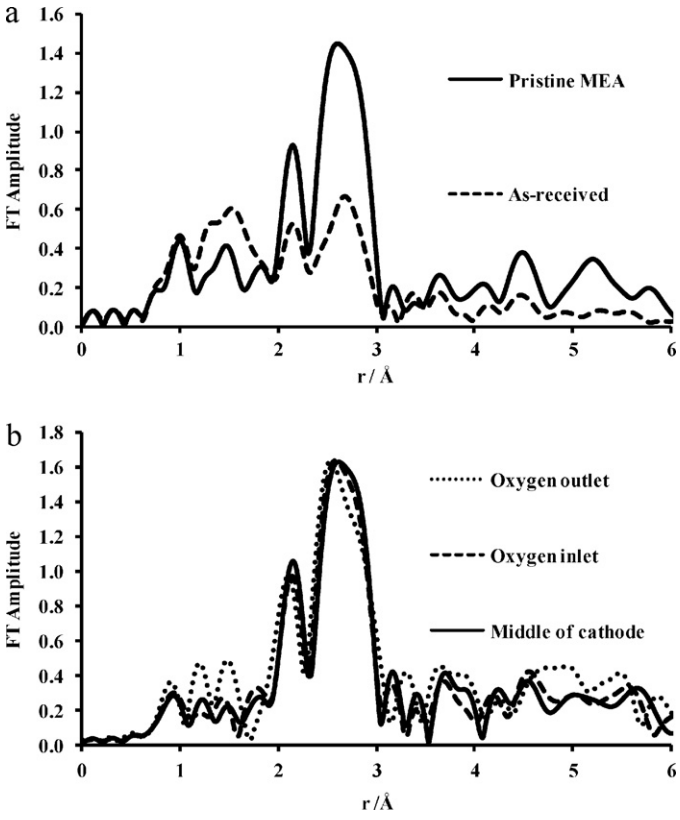

Fig. 6. FT Pt L_3 edge of the cathode side: (a) pristine MEA and as-received catalyst, (b) from different regions, i.e. oxygen inlet, middle and outlet. In good agreement with the XRD data, no site-dependent changes were observed.

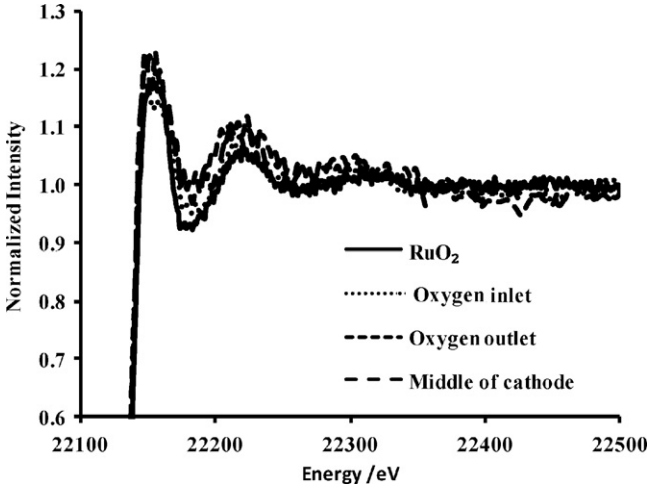

Fig. 7. Ru *K* edge XANES spectra of the cathode catalyst. Near edge characteristics similar to a RuO_2 standard were found all over the cathode side of the MEA.

Table 3
EXAFS analysis of the cathode catalyst at the Pt L_3 edge.

Pt edge	NPt–Pt	rPt–Pt (Å)	E_0Pt–Pt (eV)	NPt–O	rPt–O (Å)	E_0Pt–O (eV)
As-received	3.1	2.74	7.47	1.4	1.98	1.85
Pristine MEA	7.2	2.75	7.62	0.6	1.97	1.46
Inlet	8.1	2.75	5.48			
Middle	8.2	2.76	8.51			
Outlet	8.0	2.74	7.70			

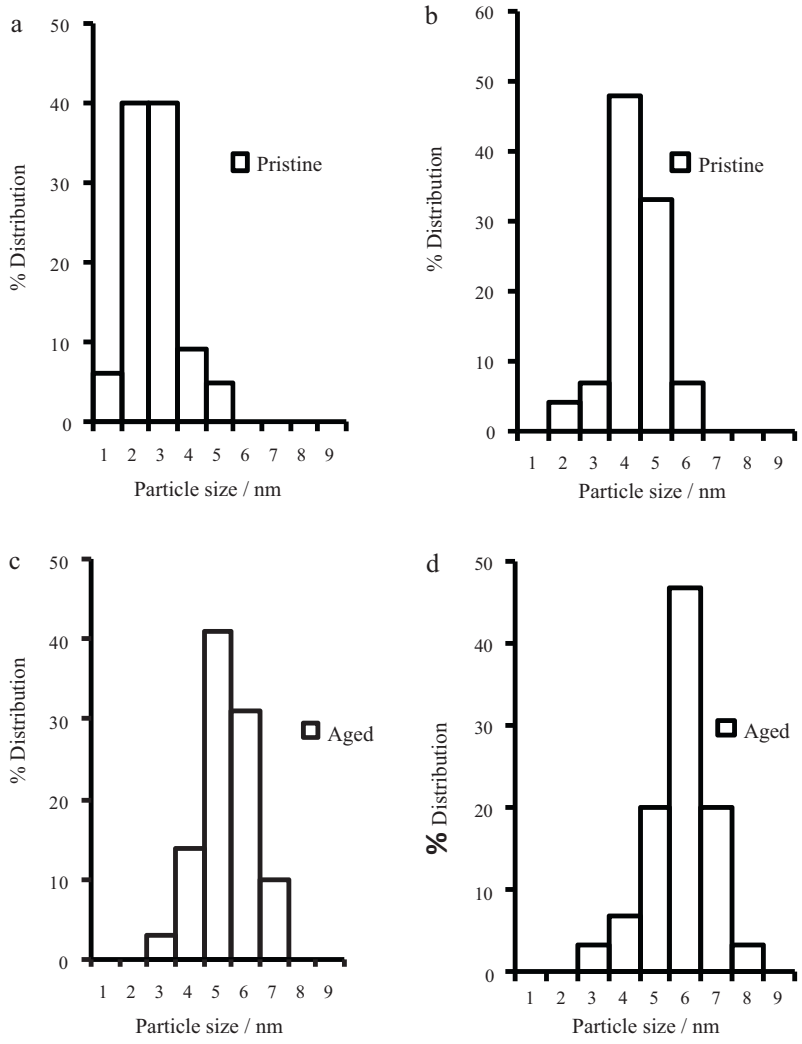

Fig. 8. Particle size distribution from thin cut TEM analysis: (a) pristine MEA anode side, (b) pristine MEA cathode side, (c) aged MEA anode side, and (d) aged MEA cathode side.

the cathode, it could be concluded that Ru is preferentially leached out from unalloyed Ru or the unreduced Ru oxides. The reduction and leaching of the oxide phase can bring alloyed particles together, and an overall increase in the particle size can be observed during operation.

Fig. 5a and b represents the FT at the Pt and the Ru edge for the aged anode catalyst from different regions in the fuel cell. An overall increase in the FT amplitude can be observed for the aged catalyst compared to the pristine catalyst, which can also be correlated with particle growth. Additional information on the nature of the ruthenium oxide can be obtained from the r_{Ru-O} bond distance (Table 2a); recent XAS investigations by Rose et al. give a correlation of the bond distance (r_{Ru-O}) with the hydrous and anhydrous form of ruthenium oxide [23]. The Ru–O bond distance obtained from the EXAFS for the as-received catalyst and the catalyst in OCV condition showed a larger bond distance of r_{Ru-O} = 2.03, which was assigned to hydrous ruthenium oxide, and is in good agreement with the Rose et al. findings. EXAFS analysis of the aged sample revealed a much smaller r_{Ru-O} bond distance for the methanol outlet in comparison to the inlet and middle region. This smaller bond distance was assigned to anhydrous ruthenium oxide, which occurs at relatively higher potentials. The preferential formation of anhydrous ruthenium oxide at the methanol outlet may be due to cell reversal and fuel starvation, which is expected to be severe at the methanol outlet [24]. It has been proposed by Rolison et al. that anhydrous ruthenium oxide is highly unfavorable for the fuel cell catalysis due to its low electron and proton conductivity [8], and thus methanol outlet regions might degrade and lose their activity faster than other regions.

The Pt L_3 EXAFS investigation of the cathode catalyst also showed a significant fraction of oxidized Pt (Table 3). In contrast to the anode catalyst, a significant increase in the coordination number was observed during the MEA preparation. The overall increase in the particle size during MEA fabrication was also reflected in the large increase in FT amplitude observed for the fresh MEA (Fig. 6a), which is also in good agreement with the XRD results. The coordination number was also found to increase after fuel cell operation, and no significant difference in the structure was observed for the different regions (Fig. 6b). Ru *K* edge measurements in fluorescence mode on the cathode catalyst at different regions gave XANES spectra, which were identical to that of a ruthenium oxide standard (Fig. 7), supporting the idea that cross over ruthenium from the anode gets dispersed everywhere in the cathode and is predominantly oxidized. It has to be amorphous, however, since it was not detected by XRD.

In order to obtain more detailed information of the whereabouts of the ruthenium in the cathode, MEA thin cuts from methanol inlet, electrode middle and outlet were analyzed using TEM. Particle size distributions after ageing were obtained and are summarized in Fig. 8. The size distributions appear rather narrow and are shifted

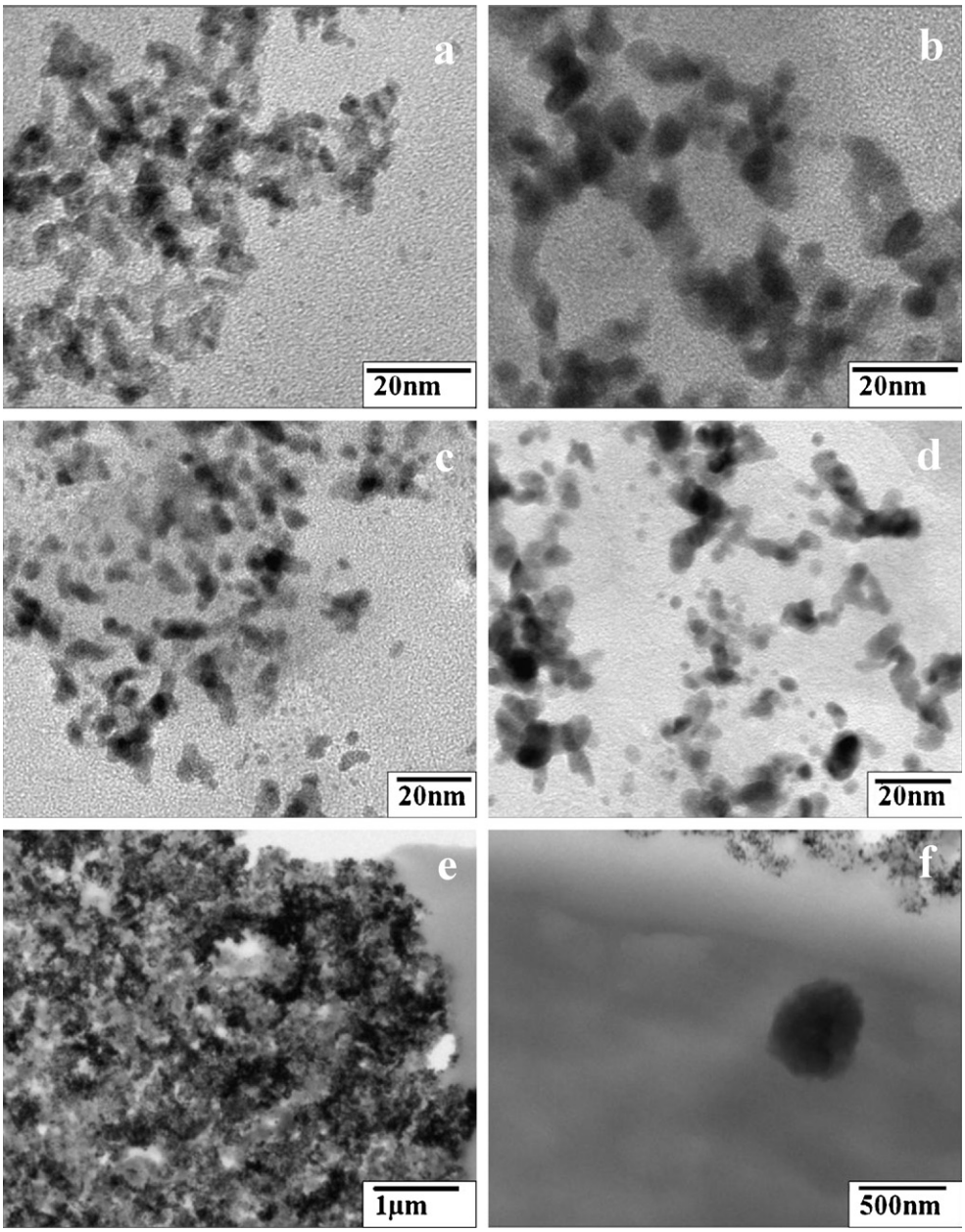

Fig. 9. TEM micrograph for: (a) pristine MEA anode side, (b) aged MEA anode side, (c) pristine MEA cathode side, (d) aged MEA cathode side, (e) low magnification image of the aged MEA, and (f) membrane electrode interface close to the cathode inlet from methanol outlet region.

to higher values for the aged MEAs. Compared to the XRD data, the average sizes by TEM analysis are slightly larger, since XRD is only sensitive to coherently scattering regions, i.e. crystalline parts. Anode and cathode sides of the MEA were distinguished by particle size and Ru content. TEM micrographs of a pristine MEA anode revealed individual particles, but also particles assembling into chain-like structures, and a distribution of particle sizes with a median value in the range of 2–3 nm (Fig. 9a). The length and number of the chain-like ensembles of nanoparticles was found to increase with ageing, while a broader distribution of particle sizes with the median value shifted to 5 nm was observed (Fig. 9b). TEM investigation of the pristine MEA cathode revealed a good dispersion of the catalyst in comparison to the anode with an average particle size of 4–5 nm. The ageing of the MEA causes these particles to form chains similar to those observed for the anode, and a broader distribution of particle sizes was observed (Fig. 9c and d). Severe aggregation was found all over the MEA after ageing, probably due to support corrosion (cathode) and dissolution of ruthenium oxide (anode) (Fig. 9e).

TEM micrographs also showed large amorphous precipitates in the membrane (Fig. 9f) predominantly at the methanol outlet regions or the cathode inlet regions (please note: operation was done in counter flow). However, the high energy of the electron beam made it nearly impossible to record EDX spectra on these particles, as the Nafion membrane was damaged by the beam. Instead, EDX mapping of a similar sample was recorded with an SEM, which also showed aggregates in the membrane. With this approach large precipitates could be identified as Ru. However, ruthenium maps of the cathode side of the electrode were less unambiguous. This is mainly due to the much weaker signals for Ru compared to the Pt as a result of the relative small amount of cross over Ru on the one hand and the generally low signal intensity collected from the thin cut samples on the other hand. However, the XANES data also gave evidence of cross over Ru homogeneously distributed all over

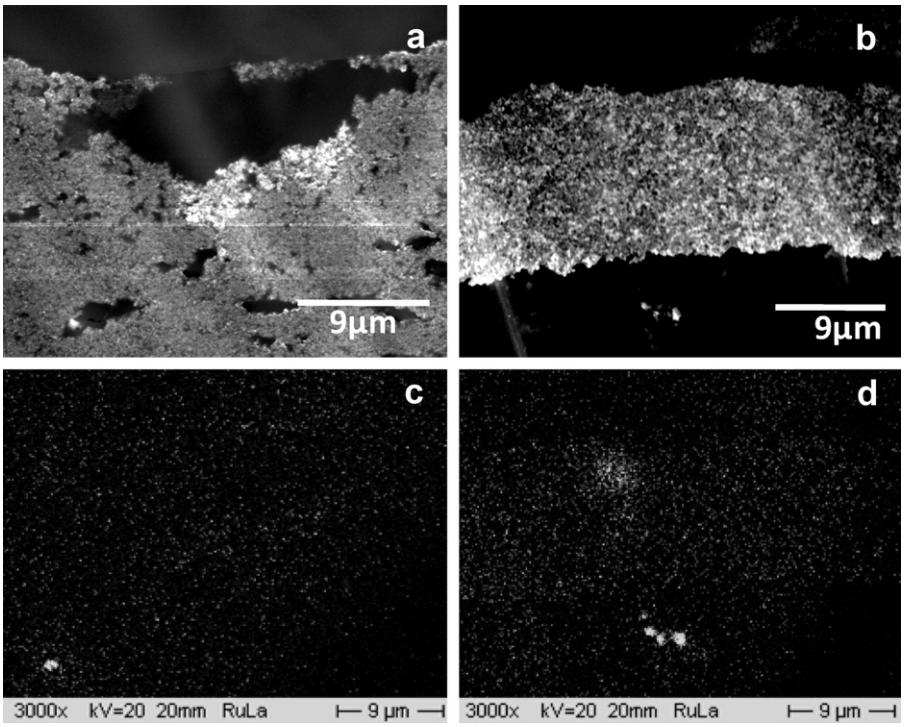

Fig. 10. EDX analysis of (a) SEM image pristine MEA anode, (b) SEM image aged anode, (c) Ru mapping pristine MEA anode, and (d) Ru mapping aged anode.

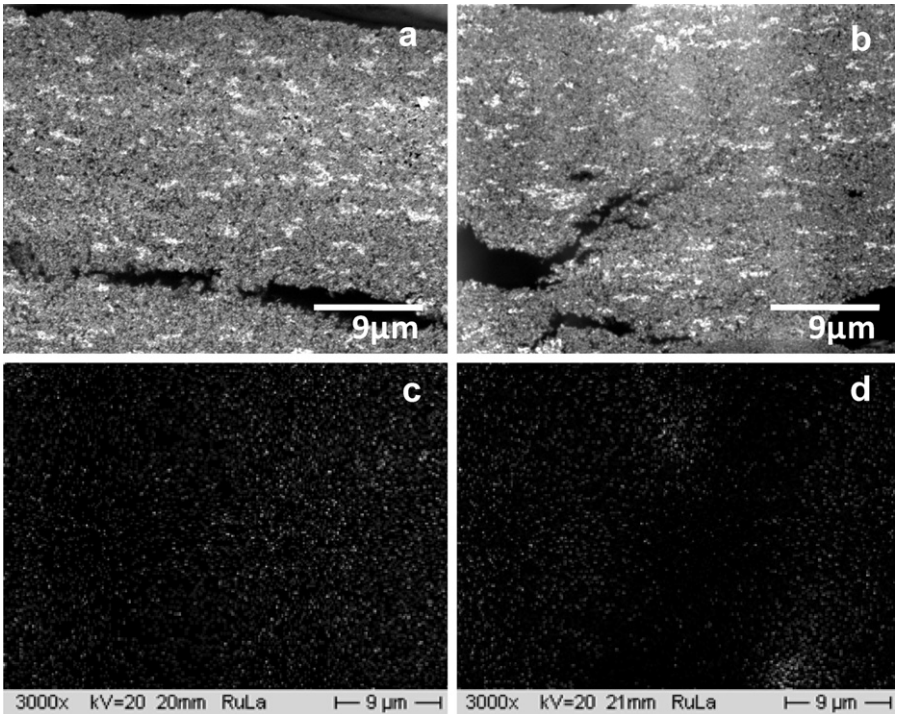

Fig. 11. EDX analysis of (a) SEM image pristine MEA cathode, (b) SEM image aged cathode, (c) Ru mapping pristine MEA cathode, and (d) Ru mapping aged cathode.

the cathode and thus corroborate the EDX findings. Detailed EDX mapping results for the aged and the fresh MEA are presented for the anode in Fig. 10 and the cathode in Fig. 11, respectively. EDX mapping was also used for Pt showing the distribution of Pt in the MEA, which was found to be more inhomogeneous for the aged than for the fresh MEA (not shown). In contrast to the H_2-PEM cell, no precipitation band of Pt was observed in the membrane in DMFC [25].

4. Conclusion

XRD, XAS, and TEM were used to investigate in detail different regions at the anode and cathode side of an MEA after a fuel cell stack test. Both anode and cathode side showed particle growth with ageing, whereas particle growth during MEA preparation was prominent only for the cathode catalyst. It was also found that ruthenium is present in the anode catalyst in three different states,

as: (a) a fraction of Ru in the Pt/Ru is oxidized, while (b) a significant fraction became reduced during fuel cell operation and (c) some Ru exists in the alloy phase. The reduction of the oxide phase can create unalloyed Ru, which is assumed to be more susceptible to dissolution and cross over to the cathode side compared to the Ru alloyed with Pt. XAS and EDX analysis of the cathode catalyst revealed the presence of well distributed oxidized Ru all over the cathode. Thus, the overall ORR activity of the cathode might be reduced due to adsorption of Ru oxides on active Pt sites, catalyzing the oxidation of cross over methanol. Although no precipitation band was observed in the membrane, TEM and EDX analysis still showed the presence of large Ru precipitates in the membrane. The preferential formation of these precipitates at the methanol outlet might be due to fuel starvation occurred during the standstill operation. XAS results also gave evidence for the presence of anhydrous ruthenium oxide at the fuel outlet regions, possibly due to the high interfacial potential occurring during the fuel starvation process. Spatially resolved in situ studies will be required to study these processes further and are under way.

Acknowledgements

The kind support of Adam Webb, beamline scientist X1 Hasylab, and technical support from Ulrike Kunz for thin cuts sample preparation and EDX mapping are gratefully acknowledged. Financial support of the BMBF under grant no. 03SF0324E is gratefully acknowledged.

References

[1] P. Piela, C. Eickes, E. Brosha, F. Garzon, P. Zelenay, J. Electrochem. Soc. 151 (2004) A2053.
[2] J.T. Wang, S. Wasmus, R.F. Savinell, J. Electrochem. Soc. 143 (1996) 1233.
[3] Z. Qi, A. Kaufman, J. Power Sources 110 (2002) 177.
[4] H. Kim, S.-J. Shin, Y.-G. Park, J. Song, H.T. Kim, J. Power Sources 160 (2006) 440.
[5] M.K. Jeon, K.R. Lee, K.S. Oh, D.S. Hong, J.Y. Won, S. Li, S.I. Woo, J. Power Sources 158 (2006) 1344.
[6] M. Watanabe, S. Motoo, J. Electroanal. Chem. 60 (1975) 275.
[7] H.A. Gasteiger, N. Markovic, P.N. Ross, E.J. Cairns, J. Phys. Chem. 97 (1993) 12020.
[8] D.R. Rolison, P.L. Hagans, K.E. Swider, J.W. Long, Langmuir 15 (1999) 774.
[9] T. Saida, W. Sugimoto, Y. Takasu, Electrochim. Acta 55 (2010) 857.
[10] C. Lai, J. Lin, K. Hsueh, C. Hwang, K. Tsay, L. Tsai, Y. Peng, J. Electrochem. Soc. 155 (2008) B843.
[11] J. Mergel, A. Glüsen, C. Wannek, Current Status of and Recent Developments in Direct Liquid Fuel Cells, in: Hydrogen and Fuel Cells, in: D. Stolten (Eds.), Wiley-VCH Verlag, Weinheim, pp. 41–60.
[12] P. Scherrer, Nachr. Ges. W iss 26 (1918) 98.
[13] C. Roth, N. Martz, Th. Buhrmester, H. Fuess, Phys. Chem. Chem. Phys. 4 (2002) 3555.
[14] B. Ravel, M. Newville, J. Synchrotron Radiat. 12 (2005) 537.
[15] M. Newville, P. Livins, Y. Yacoby, J.J. Rehr, E.A. Stern, Phys. Rev. B 47 (1993) 14126.
[16] F. Scott, S. Mukerjee, D.E. Ramaker, J. Electrochem. Soc. 154 (2007) A396.
[17] D.A. Blom, J.R. Dunlap, T.A. Nolan, L.F. Allard, J. Electrochem. Soc. 150 (2003) A414.
[18] A.S. Arico, P. Creti, H. Kim, R. Mantegna, N. Giordano, V. Antonucci, J. Electrochem. Soc. 143 (1996) 3950.
[19] H. Nitani, T. Nakagawa, H. Daimon, Y. Kurobe, T. Ono, Y. Honda, A. Koizumi, S. Seino, T.A. Yamamoto, Catal. Appl. A 326 (2007) 194.
[20] S.Q. Song, Z.X. Liang, W.J. Zhou, G.Q. Sun, Q. Xin, V. Stergiopoulos, P. Tsiakaras, J. Power Sources 145 (2005) 495.
[21] A.I. Frenkel, C.H. Hills, R.G. Nuzzo, J. Chem. Phys. B 105 (2001) 12689.
[22] A.E. Russell, A. Rose, Chem. Rev. 104 (2004) 4613.
[23] A. Rose, E.M. Crabb, Y. Qian, M.K. Ravikumar, P.P. Wells, R.J.K. Wiltshire, J. Yao, R. Bilsborrow, F. Mosselmans, A.E. Russell, Electrochim. Acta 52 (2007) 5556.
[24] D. Liang, Q. Shen, M. Hou, Z. Shao, B. Yi, J. Power Sources 194 (2009) 847.
[25] F. Ettingshausen, J. Kleemann, M. Michel, M. Quintus, H. Fuess, C. Roth, J. Power Sources 194 (2009) 899.